BARC/1999/E/022

BARC/1999/E/022

भारत सरकार
GOVERNMENT OF INDIA
भाभा परमाणु अनुसंधान केन्द्र
BHABHA ATOMIC RESEARCH CENTRE

EXPERIMENTAL TECHNIQUES IN NUCLEAR PHYSICS

by

R. K. Choudhury
Nuclear Physics Division

1999

BARC/1999/E/022

BARC/1999/E/022

GOVERNMENT OF INDIA
ATOMIC ENERGY COMMISSION

EXPERIMENTAL TECHNIQUES IN NUCLEAR PHYSICS

by
R.K. Choudhury
Nuclear Physics Division

BHABHA ATOMIC RESEARCH CENTRE
MUMBAI, INDIA
1999

BIBLIOGRAPHIC DESCRIPTION SHEET FOR TECHNICAL REPORT
(as per IS : 9400 - 1980)

01	*Security classification :*	Unclassified
02	*Distribution :*	External
03	*Report status :*	New
04	*Series :*	BARC External
05	*Report type :*	Technical Report
06	*Report No. :*	BARC/1999/E/022
07	*Part No. or Volume No. :*	
08	*Contract No. :*	
10	*Title and subtitle :*	Experimental techniques in nuclear physics
11	*Collation :*	38 p., 12 figs., 4 tabs.
13	*Project No. :*	
20	*Personal author(s) :*	R. K. Choudhury
21	*Affiliation of author(s) :*	Nuclear Physics Division, Bhabha Atomic Research Centre, Mumbai
22	*Corporate author(s) :*	Bhabha Atomic Research Centre, Mumbai - 400 085
23	*Originating unit :*	Nuclear Physics Division, BARC, Mumbai
24	*Sponsor(s) Name :*	Department of Atomic Energy
	Type :	Government

Contd... (ii)

30	*Date of submission :*	August 1999
31	*Publication/Issue date :*	September 1999
40	*Publisher/Distributor :*	Head, Library and Information Services Division, Bhabha Atomic Research Centre, Mumbai
42	*Form of distribution :*	Hard copy
50	*Language of text :*	English
51	*Language of summary :*	English
52	*No. of references :*	12 refs.
53	*Gives data on :*	
60	*Abstract :* A variety of experimental techniques involving wide varieties of nuclear radiation detection methods are required to carry out research in different areas of nuclear physics. The progress in the design and operation of nuclear radiation detectors in various applications has been very rapid and a periodic review in this field is always appropriate. The present report, while dealing with the general principles of particle and radiation detection using conventional detectors of gas, scintillator and semiconductor types, also gives an update of the recent developments in sophisticated detector systems which are built to meet the requirements of present day nuclear physics experiments.	
70	*Keywords/Descriptors :* CHERENKOV COUNTERS; SHOWER COUNTERS; ELECTROMAGNETIC RADIATION; PARTICLE INTERACTIONS; PHOTONS; NEUTRONS; STOPPING POWER; IONIZATION CHAMBERS; PROPORTIONAL COUNTERS; SCINTILLATION COUNTERS; SPECIFICATIONS; PARTICLE IDENTIFICATION; SEMICONDUCTOR DETECTORS	
71	*INIS Subject Category :*	E4130
99	*Supplementary elements :*	

EXPERIMENTAL TECHNIQUES IN NUCLEAR PHYSICS

R.K. CHOUDHURY

ABSTRACT

A variety of experimental techniques involving wide varieties of nuclear radiation detection methods are required to carry out research in different areas of nuclear physics. The progress in the design and operation of nuclear radiation detectors in various applications has been very rapid and a periodic review in this field is always appropriate. The present report, while dealing with the general principles of particle and radiation detection using conventional detectors of gas, scintillator and semiconductor types, also gives an update of the recent developments in sophisticated detector systems which are built to meet the requirements of present day nuclear physics experiments.

CONTENTS

EXPERIMENTAL TECHNIQUES IN NUCLEAR PHYSICS

R. K. CHOUDHURY

1 Introduction

Progress in experimental nuclear and particle physics has been closely associated with the developments in the accelerator and detector technologies. Presently, with the use of large accelerator facilities, it has been possible to achieve centre mass energies upto a few hundred GeV/nucleon either in fixed target accelerators or with collider beams, which enables one to investigate the unexplored regions of nuclear phenomena. Accelerator based experiments are planned depending on the ability of the researcher to detect and characterize the particles produced in the collisions of the target and projectile nuclei.With increasing bombarding energy the complexity of the heavy ion collisions increases as one can see from the pictures (shown in fig.1) of some typical collisions in the high energy heavy ion experiments . In order to cope with the increasing demands of the experiments for higher detection capabilities in terms of sensitivity and better resolution, the detection equipments have undergone major developments in many different aspects.The developments have taken place in (i) the size and complexity of the detection system (ii) the speed of data collection, (iii) the versatility of the detector techniques (iv) the reliability of the equipment through innovations in fast on-line control and monitoring of the experimental set up. The present series of lectures is aimed at providing some discussions on the basic concepts of the detection methods and the techniques used in the experimental setups at intermediate and relativistic energies.

2 Principles of particle detection

Before a particle can be detected, it must first undergo some sort of interaction with the material of a detector. Electromagnetic interactions are the most important of all processes for particle detection. Other type of interactions such as strong and weak nuclear interactions are important for detection of neutral particles.

2.1 Interaction of charged particles with matter

We will begin by considering the kinetic energy loss of an incident charged particle due to its Coulomb interaction with the charged particles in matter. Let the incident particle have mass m_1, charge z_1e and velocity v_1. We assume it to interact with a particle in the material with mass m_2 and charge Z_2e and that the material particle is at rest. The moving charge creates an electric and magnetic field at the location of the material particle. The magnetic interaction is not important, since the material particle is essentially at rest. The changing

electric field of the moving particle gives a net impulse to the material particle and imparts a momentum

$$\Delta p = \frac{2z_1 z_2 e^2}{v_1 b} \tag{1}$$

where b is the impact parameter of interaction. The energy transfer can be written as

$$\Delta E = \frac{\Delta p^2}{2m_2} = \frac{2z_1^2 z_2^2 e^4}{b^2 v_1^2 m_2}$$

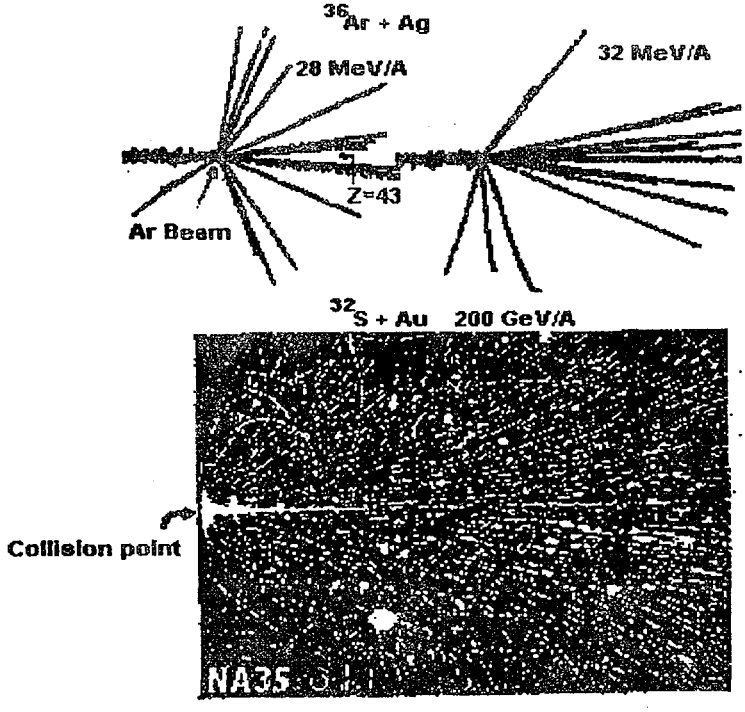

Figure 1: Typical pictures of particle tracks in nucleus-nucleus collisions

It can be seen from above that the electrons of the medium are the major contributors to the energy loss and not the nuclei. ($z_2 = Z \sim A/2, m_2 = A\ m_p/m_e$, *for the nuclei*). So we can substitute $z_2 = 1$ and $m_2 = m_e$ in the above equation. The total energy loss per unit length of the material can be calculated by integrating the above equation over all impact parameters and by considering the total number of electrons per unit volume

$$\frac{dE}{dx} = \frac{-2\pi z_2 N_A \rho}{A} \frac{2z_1^2 e^4}{m_e v^2} \int_{b_{min}}^{b_{max}} \frac{db}{b} \tag{2}$$

Here z_2 is the nuclear charge of the atom of the medium, N_A=Avogadro number and ρ is the density of the medium.

In the classical treatment by Bohr [1] the energy loss was evaluated by evaluating the integration limits classically. A more rigorous quantum mechanical treatment was given

by Bethe and Bloch [2], where the energy loss was calculated by classifying the collisions as distant and close collisions depending on the amount of energy transfer involved. For distant collisions, the incident particle interacts with the atom as a whole and causes excitation of an electron to a higher energy level or ionisation. For close collisions, the interaction can be considered to be with free electrons and the energy loss is calculated using the appropriate interaction crosssection. The total energy loss is the sum of the contributions from close and distant collisions and is given by

$$\frac{dE}{dx} = -\frac{4\pi n_e z_1^2 e^4}{m_e v_1^2}[\ln(\frac{2m_e v^2\gamma^2}{I}) - \beta^2] \tag{3}$$

where $n_e = z_2 N_A \frac{\rho}{A}$
or

$$\frac{dE}{dx} = -Kn_e(\frac{z_1}{\beta})^2[\ln(\frac{2m_e c^2\beta^2\gamma^2}{I}) - \beta^2] \tag{4}$$

where

$$K = 4\pi(\frac{e^2}{m_e c^2})^2 m_e c^2 = 5.0989 \times 10^{-25} MeVcm^2 \tag{5}$$

$\gamma = (1-\beta^2)^{-\frac{1}{2}}$ and $\beta = \frac{v_1}{c}$

Now let us consider the important features of the above equation. The energy loss depends quadratically on the charge and velocity of the particle but not on its mass. The medium dependence comes linearly through n_e and logarithmically through mean ionisation potential I. As the velocity of the particle increases from near zero, dE/dx falls as $1/v^2$, goes through a minimum with $dE/dx \sim 2MeV/(g/cm^2)$ for $\beta\gamma \approx 3$ and then continues to increase due to the $\ln\gamma^2$ factor. However, at very large values of γ, there is a density effect due to dielectric screening of projectiles electric field, causing the energy loss to nearly saturate for large values of $\beta\gamma(\geq 100)$. Taking the density effect into account, the energy loss formula can be written as

$$\frac{dE}{dx} = -5.0989 \times 10^{-25} n_e(\frac{z_1}{\beta})^2[\ln(\frac{2m_e c^2\beta^2\gamma^2}{I}) - \beta^2 - \frac{\delta(\gamma)}{2}] \;\; MeV/cm \tag{6}$$

It may also be noted that at low energies ($\frac{E}{m} < 1 - 2MeV/n$), the charge of the particle cannot be considered as bare nuclear charge due to the recombination of electrons and the ionic charge (z_{eff}) comes into play for calculating the energy loss. A simple relationship for the effective charge is given by

$$z_{eff} = z_1(1 - A\exp(-Bv_R))$$

where v_R is defined as the ratio of the ion velocity to the Thomas-Fermi electron velocity ($v_R = v/v_0 z^{\frac{2}{3}}$), v_0 being the orbital velocity of the electron in the first Bohr orbit. Due to the effective charge, the energy loss decreases again at low particle energies.

The essential features of the energy loss of charged particles in a medium can be seen from fig.2, where we have shown the normalised energy loss $\frac{1}{z_1^2}$(dE/dx) as a function

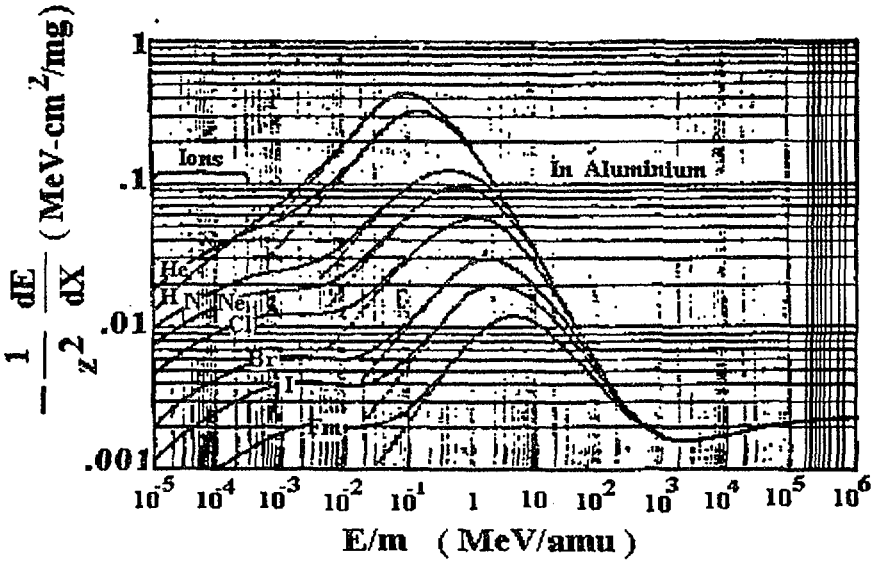

Figure 2: Stopping power curves for various heavy ions

of E/m for a number of heavy ions in aluminium over a wide energy region. At very low energies, there is an additional "nuclear" contribution to the energy loss due to energy transfer to screened nuclei of the medium as shown by the deviation of the total stopping power (continuous line) from the electronic part (dashed line). At very high velocities, there is a universal behaviour of the energy loss for all the ions as expected from eq.(6) above.

2.1.1 Range of a particle

The range represents the distance transversed by a particle along its trajectory.

$$R(E) = \int_E^0 \frac{1}{-\frac{dE}{dx}} dE \tag{7}$$

let us write $\frac{dE}{dx} = z_1^2 f(v) = z_1^2 f(\frac{E}{m})$
hence

$$R(\frac{E}{m}) = \int \frac{1}{z_1^2 f(\frac{E}{m})} m \frac{dE}{m} = \frac{m}{z_1^2} g(\frac{E}{m}) \tag{8}$$

where g is a universal function of E/m. From above one can write the scaling law for range as

$$R_2(\frac{E_2}{m_2}) = \frac{m_2 z_1^2}{m_1 z_2^2} R_1(\frac{E_2}{m_2}) \tag{9}$$

Hence if the range of some particle (say proton) is known as a function of v or E/m, one can obtain the range of another particle of any given energy using the above relationship. A simple empirical expression for the range energy relationship of proton is

$$R(E) = (\frac{E}{E_0})^n \tag{10}$$

where range is measured in meters, and E_0 = 9.3 MeV, n = 1.8 for protons in air, which can be used handily to evaluate the range of other particles in air.

2.1.2 Energy loss in mixtures and compounds

For mixtures and compounds, one can write

$$\frac{1}{\rho}(\frac{dE}{dx})_m = \Sigma a_i A_i (\frac{dE}{dx})_i \tag{11}$$

where, a_i= Number of atoms of i^{th} element,
A_i = Atomic weight of i^{th} element,
$A_m = \sum_i a_i A_i$, is the total atomic weight , and
ρ= density of mixture or compound

One can also define effective values of different quantities and use them in the original formula (6) as :

$Z_{eff} = \sum_i a_i Z_i$ $A_{eff} = \sum_i a_i A_i$
$\delta_{eff} = \sum_i \frac{a_i Z_i \delta_i}{Z_{eff}}$, $\ln I_{eff} = \sum_i \frac{a_i Z_i \ln I_i}{Z_{eff}}$

2.2 Interaction of electrons and positrons with matter

Electrons and positrons lose energy by ionization and excitation during the collision with electrons in the medium just as other heavier charged particles. However, because of their small mass, they also lose energy due to production of bremsstrahlung radiation during acceleration or deceleration process in the vicinity of the atoms of the medium. The total energy loss for electrons and positrons, therefore, is composed of two parts

$$(\frac{dE}{dx})_{tot} = (\frac{dE}{dx})_{rad} + (\frac{dE}{dx})_{coll} \tag{12}$$

2.2.1 Collisional loss

The total energy loss for electrons and positrons, due to collisions with electrons of the medium, is given by the following expressions :

$$\frac{dE}{dx}_{e^+,e^-} = \frac{2\pi n_e r_e^2 m_e c^2}{\beta^2}[\ln \frac{(\tau^2(\tau+2))}{2(\frac{I}{m_e c^2})^2} + F(\tau) - \delta] \tag{13}$$

where

$\tau = \frac{T}{m_e c^2}$, T=kinetic energy of e^- or e^+

and

$$F(\tau) = (1-\beta^2) + \frac{\frac{\tau^2}{8} - (2r_e+1)\ln 2}{(\tau+1)^2}, \quad \text{for } e^-$$
$$= 2\ln 2 - \frac{\beta^2}{12}(23 + \frac{14}{\tau+2} + \frac{10}{(\tau+2)^2} + \frac{4}{(\tau+2)^3}), \quad \text{for } e^+$$

The difference between e^- and e^+ arises due to use of Moller and Bhabha scattering crosssection for the collisions for the two cases.

2.2.2 Bremsstrahlung loss

The radiation loss depends on the bremsstrahlung emission probability which varies as inverse square of particle mass

$$\sigma \ \alpha \ r_e^2 = (\frac{e^2}{mc^2})^2$$

The radiation loss by heavy particles such as muons (m~106 MeV) is 40000 times lower than that for electrons.

Since bremsstrahlung emission depends on the strength of the electric field felt by the electron, the amount of screening of the nuclear charge by the atomic electrons plays an important role. The effect of screening can be parametrized by the quantity as

$$\xi = \frac{100 m_e c^2 (E_0 - E)}{E_0 E Z^{\frac{1}{3}}} \tag{14}$$

where $(E_0 - E) = h\nu$ = energy of photon, E_0= initial energy, E = final energy of electron.

When $\xi \longrightarrow 0, h\nu \longrightarrow 0$: complete screening

$\xi \longrightarrow \infty, h\nu \longrightarrow E_0$: No screening

For relativistic energies, E_0 > a few MeV, the bremsstrahlung crosssection due to nuclear charge, Z is given by

$$d\sigma = 4Z^2 r_e^2 \frac{e^2}{\hbar c}\frac{d\nu}{\nu}[(1+\epsilon^2)(\frac{\phi_1(\xi)}{4} - \frac{\ln Z}{3} - f(Z)) - \frac{2\epsilon}{3}(\frac{\phi_2(\xi)}{4} - \frac{\ln Z}{3} - f(Z))] \tag{15}$$

where $\epsilon = E/E_0$, f(Z) = Coulomb correction and ϕ_1, ϕ_2 are the screening functions.

In the limiting cases of no screening and complete screening, one can write simpler analytic forms for the bremstrahlung crosssection as

i) No screening ($\xi >> 1$)

$$d\sigma = 4Z^2 r_e^2 \frac{e^2}{\hbar c}\frac{d\nu}{\nu}(1+\epsilon^2-\frac{2\epsilon}{3})[\ln(\frac{2E_0E}{m_ec^2h\nu})-\frac{1}{2}-f(Z)] \tag{16}$$

ii) Complete screening ($\xi = 0$)

$$d\sigma = 4Z^2 r_e^2 \frac{e^2}{\hbar c}\frac{d\nu}{\nu}[(1+\epsilon^2-\frac{2\epsilon}{3})(\ln(183Z^{-\frac{1}{3}})-f(Z))+\frac{\epsilon}{9}] \tag{17}$$

The energy loss due to radiation can be written as

$$-(\frac{dE}{dx})_{rad} = \frac{\rho N_A}{A}\int_0^{\nu_0} h\nu\frac{d\sigma(E_0,\nu)}{d\nu}d\nu = NE_0\phi_{rad}; \phi_{rad} = \frac{1}{E_0}\int_0^{\nu_0} h\nu\frac{d\sigma(E_0,\nu)}{d\nu}d\nu \tag{18}$$

Since $\frac{d\sigma}{d\nu} \alpha \frac{1}{\nu}$, one can see that ϕ_{rad} is practically independent of ν and is a function of material only.

Again, one can write

for $\xi \gg 1$, $\phi_{rad} = 4Z^2 r_e^2 \frac{e^2}{\hbar c}[\ln(\frac{2E_0}{m_ec^2})-\frac{1}{3}-f(Z)]$ and

for $\xi = 0$, $\phi_{rad} = 4Z^2 r_e^2 \frac{e^2}{\hbar c}[\ln(183Z^{-\frac{1}{3}})-\frac{1}{18}-f(Z)]$

For $e-e$ bremsstrahlung due to atomic electrons, Z^2 is replaced by Z and so one can take this contribution into account by replacing $Z^2$by Z(Z+1) in above equations. In fig.3, we show the relative importance of the two types of energy losses for the electrons as a function of the energy.

It is seen that for electrons at higher energies, the bremsstrahlung loss takes completely over the ionisation loss. One can define the critical energy,E_c at which

$$(\frac{dE}{dx})_{rad} = (\frac{dE}{dx})_{coll}$$

An approximate formula for E_c due to Bethe [3] is given by

$$E_c \simeq 1600\frac{m_ec^2}{Z} \tag{19}$$

Another quantity of interest in dealing with radiation loss is the radiation length. One sees that at very high energies, $\frac{dE}{dx} = -NE\phi_{rad}$ or $\frac{dE}{E} = -N\phi_{rad}dx$

Integrating, we get

$$E = E_0\exp(-xN\phi_{rad}) = E_0\exp(-\frac{x}{L_{rad}}), \quad \text{where } L_{rad} = \frac{1}{N\phi_{rad}}$$

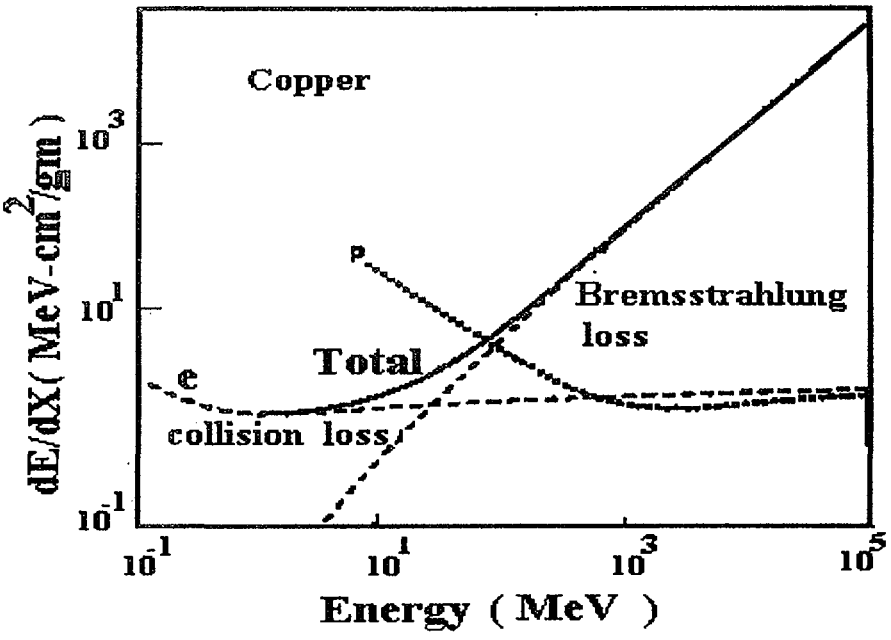

Figure 3: Radiation loss Vs Collision loss for electrons in Copper

Hence, the radiation length L_{rad} can be defined as the length of material required to reduce the energy of electron by $1/e$ of the original value. Material thickness is usually measured in unit of radiation length so that radiation energy loss per unit thickness ($t = x/L_{rad}$) is roughly independent of material type. In table 1, we give the values of E_c and L_{rad} for some of the commonly used materials in detector fabrication.

Material	$E_c(MeV)$	L_{rad}	
		cm	$\frac{gm}{cm^2}$
Air	102	30050	36.2
H_2O	92	36.1	36.08
Organic Scint.	105	42.4	43.8
Polyesterene	109	42.9	43.8
Al	51	8.9	24.01
Cu	24.8	1.43	12.86
Pb	9.51	0.56	6.37
Fe	27.4	1.76	13.84
BGO($BiGe_3O_{12}$)	13.1	1.12	7.98
BaF_2	17.8	2.05	9.91
NaI	17.4	2.59	9.49

Table 1.

From this table one can determine the effectiveness of different materials in stopping the high energy electrons.

2.3 Interaction of photons with matter

Photon interactions are different from that of charged particles in the sense that there is a large probability that an interacting photon can be removed from the beam. There are three major processes by which photons interact with matter : i) Photo-electric ii) Compton scattering and iii) Pair production.

The Photo-electric crosssection is given by

$$\frac{d\sigma}{d\Omega_{ph}} = 4(\frac{e^2}{\hbar c})^4\sqrt{2}Z^5\frac{8\pi r_e^2}{3}(\frac{m_e c^2}{h\nu})^{\frac{7}{2}}\ per\ atom \approx \frac{Z^5}{E_\gamma^{3.5}} \tag{20}$$

At very low energy, the photo-electron is emitted at 90^0 to photon direction, but as the photon energy increases, the emission becomes more and more forward peaked.

In Compton scattering, the incident photon gets scattered by a free electron of the atom imparting it certain energy and coming out with a reduced energy. The differential crosssection for scattering is given by the Klein-Nishina formula as [3] :

$$\frac{d\sigma}{d\Omega} = \frac{r_e^2}{2}\frac{1}{[1+\frac{h\nu}{m_e c^2}(1-\cos\theta)]^2}[1+\cos^2\theta+\frac{(\frac{h\nu}{m_e c^2})^2(1-\cos\theta)^2}{1+\frac{h\nu}{m_e c^2}(1-\cos\theta)}]$$

The total crosssection is given by

$$\sigma_{compton}\ \alpha\ \frac{Z}{h\nu_0} \tag{21}$$

The maximum energy of electron allowed by kinematics is when the photon is scattered by 180^0 and is given by

$$T_{max} = h\nu\frac{2\frac{h\nu}{m_e c^2}}{1+\frac{2h\nu}{m_e c^2}} \tag{22}$$

The Compton scattering gives a continuous distribution of electron energy with the above maximum called the Compton edge. For photon energies much greater than $m_e c^2$, the Compton edge comes about $m_e c^2/2$ less than the photopeak energy.

In pair production, the photon energy is converted to the toal energy of an electron-positron pair. Pair production is similar to the bremsstrahlung emission and involves similar screening parameter. The total pair production crosssection for the two extreme cases of screening is given by

i) No screening ($\xi >> 1$) (low energy)

$$\sigma_{pair} = 4Z^2\frac{e^2}{\hbar c}r_e^2[\frac{7}{9}[\ln(\frac{2h\nu}{m_e c^2}) - f(Z)] - \frac{109}{54}] \tag{23}$$

ii) Complete screening ($\xi \longrightarrow 0$) (high energy)

$$\sigma_{pair} = 4Z^2\frac{e^2}{\hbar c}r_e^2[\frac{7}{9}[\ln(183Z^{-\frac{1}{3}}) - f(Z)] - \frac{1}{54}] \tag{24}$$

Pair production in the field of electrons goes as Z instead of Z^2 and hence the total crosssection can be obtained by replacing Z^2 by Z(Z+1) in the above equations.

The mean free path for pair production can be obtained as

$$\lambda_{pair} = \frac{1}{N\sigma_{pair}} \approx \frac{9}{7} L_{rad}$$

which is close to the radiation length discussed above.

The total mass attenuation coefficient for the gamma rays can be written as

$$\mu = \frac{N_A \rho}{A} \sigma_{tot} = \frac{N_A \rho}{A} (\sigma_{ph} + \sigma_{comp} + \sigma_{pair}) \tag{25}$$

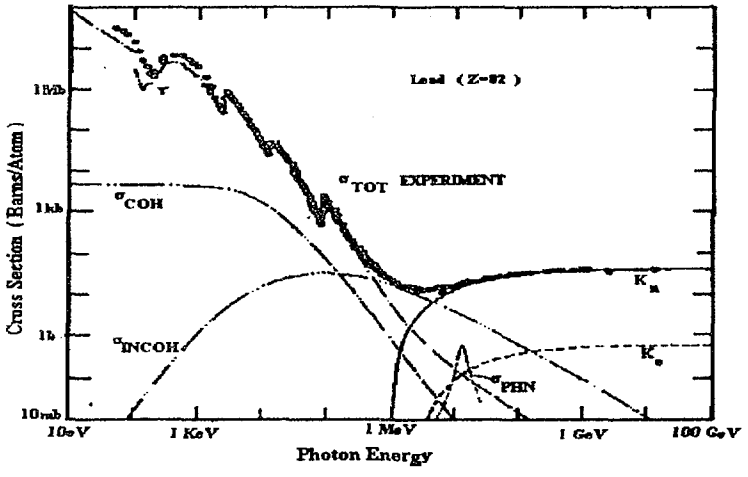

Figure 4: Crosssection Vs Energy of different photon interactions

Fig.4 shows the typical crosssections for all the above processes as a function of photon energy in lead. It can be seen that at low energies ($h\nu \leq 1.0 MeV$) the photoelectric process is the dominant process and for photons with a few MeV and higher the pair production becomes the most dominant.

2.4 Interaction of neutrons with matter

The principal means of interaction of neutrons with matter is through the strong force with the nuclei in the medium. Variety of nuclear processes takes place in these interactions :

1. Elastic scattering, A (n,n) A
2. Inelastic scattering, A(n,n)A*
3. Radiative neutron capture, A(n,γ) A+1

4. Nuclear reactions, (n,p), (n,d), (n,α) ..... (n, fission)

The total crosssection is given by sum of all these crosssections:

$$\sigma_{tot} = \sigma_{el} + \sigma_{inel} + \sigma_{cap} + \sigma_{reaction}$$

There are strong variations of σ_{tot} with energy of neutron, A and Z of the nucleus of the medium. At low energies, the capture crosssection goes as $1/v$, but at somewhat higher energies, there can be strong resonances corresponding to the nuclear levels in the compound nucleus. For low A nuclei, the scattering is the dominant mode for stopping the neutrons through moderation. Both the processes of scattering and reactions are used in the detector media to detect the neutrons.

3 Particle detectors

All particle detectors are based on the fundamental principle that the transfer of part or all of the radiation energy in the detector material is converted into some other form more accessible to human perception. The form in which the converted energy appears depends on the detector and its design. In gaseous and semiconductor detectors the ionisation process leads to some sort of current signal, while in scintillation detectors the interactions lead to emission of light. Similarly in photographic emulsions and nuclear track detectors, the ionisation induced effects lead to formation of an image of the track. The first consideration of a detector is its sensitivity, i.e. its capability to produce a usable signal for a given type of radiation and energy. The second consideration is its resolution in determination of particle type and energy. We shall briefly describe in this section the principles behind different types of detectors used in the nuclear and particle physics experiments.

3.1 Gas detectors

Gas ionisation detectors were the first electrical devices developed for radiation detection during the 1940's. With the development of scintillation and semiconductor detectors in the 1950's and 1960's, the use of gas detectors were on the wane. However, during late sixties, the development of multiwire chambers and also the advent of heavy ion accelerators for the study of heavy ion reactions saw a renewed interest in the use of gas detectors in the nuclear physics experiments. Gas detectors offer several advantages over other types of detectors. These are (i) Versatility in the size, shape of the detector (ii) no radiation damage (iii) Control on effective detector thickness by varying the gas pressure (iv) multiple mode of operation and pulse readout procedure, and (v) fairly good resolution and linearity in energy and position determination of the interacting particle etc. We shall briefly discuss the different types of gas detectors that are used in the experimental set ups in nuclear physics experiments.

3.1.1 Parallel plate ionisation chamber

Simplest among the gas detectors is the parallel plate gas ionisation chamber, in which a uniform electric field is applied across the sensitive gas volume. The interaction of a charged particle in the gas volume creates electron-ion pairs due to the ionization process. The average energy, ω , required to produce an electron-ion pair is about 30 ev in most gases. The energy resolution due to the statistical spread in the e-i pairs can be calculated as follows.

Let E be the energy of the particle absorbed in the gas volume. Then the number of e-i pairs in $N = E/\omega$ and the variance in this number is $\sigma^2 = FN$, where F is called the Fano factor, which is about 0.2 for most gases.

$$Resolution = \frac{\sigma}{E} = \sqrt{\frac{F\omega}{E}} \quad or \quad \sigma = \sqrt{FE\omega} \tag{26}$$

However, the experimental energy resolution is much higher than σ due to other spreads caused by the noise in the electronics used for processing the signals from the detector.

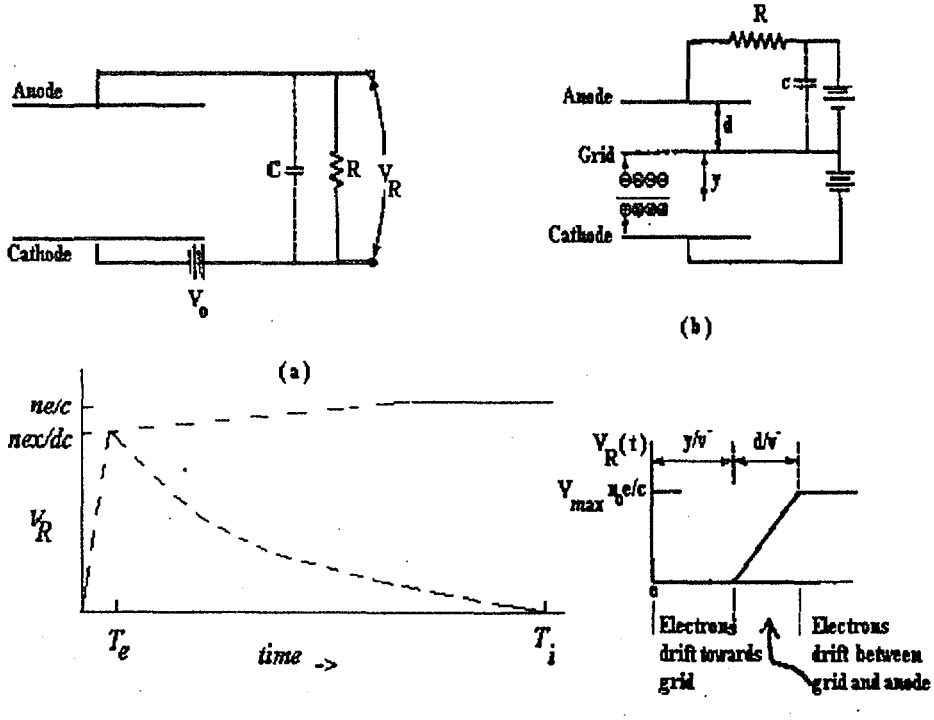

Figure 5: a.Ionisation Chamber 5: b.Gridded Ionisation Chamber

The electrons and ions move in the electric field towards the respective electrodes, where the signal is induced due to the movement of these charges. Since the electron mobility is about 10^3 times larger than ion mobility, the electronic part of the signal is induced in a much faster time scale than the ionic part. Normally the pulses from the ionization chambers are derived at the anode from the electronic part of the signal, due to which the signal height becomes dependent on the distance of the particle track from the anode. In order to make the anode pulse height independent of the distance, one introduces a grid or wire plane called Frisch grid between the cathode and anode as shown in fig.6. In this case the anode pulse height is developed only when electrons cross the Frisch grid and hence the pulse height is independent of the position of the particle track in the cathode-grid region.The pulse height at anode in then proportional to the charge released by ionization in the grid-cathode region. The output pulse characteristics in the parallel plate ionisation chambers are also shown in fig.5. Table 2 gives the values for the drift velocities of electrons, ions, the ionization potentials and mean energy per e-i pair in some typical gases used in the ionization chambers. It should be noted that the electron mobility in gases is not a constant quantity but depends on the electric field and pressure in a complex way, whereas the the most commonly used gas in ionization chambers is the P10 gas consisting of 90% Argon and 10% methane, which has very good electron mobility and much less electron attachment in atoms, thereby providing a good collection efficiency for the ionization electrons. The typical electric field applied is between 1 to 2 kilovolt/cm/atm. for proper collection of the ionization charges in the ionization chamber. It may be noted that the electron mobilities are greatly affected with mixing up of a small amount of additional gases.

Gas	Ion.Pot. (eV)	Mean energy (eV)	Ion drift velocity in (cm/s) at 1 kV/cm at 1 atm	Electron drift velocity in (cm/s) at 1 kV/cm at 1 atm
Ar	15.8	26	1.7×10^3	0.5×10^6
CO_2	13.7	33	1.09×10^3	0.7×10^6
CH_4	13.1	28	2.26×10^3	12.5×10^6
C_4H_{10}	10.8	23	0.61×10^3	10×10^6
H_2	15.4	37	13×10^3	-
He	24.6	41	10.2×10^3	-

Table 2.

3.1.2 Proportional counters

Proportional counters are made with cylindrical field configurations using a thin wire as the anode. Due to very large electric fields near the anode wire, the primary ionization electrons gain sufficient energy from acceleration to again ionize gas molecules leading to electron multiplication. If λ is the mean free path of the electron for a secondary ionizing collision, then $\alpha = 1/\lambda$ is the probability of secondary ionization per unit path length. α is called the first Townsend coefficient. The multiplication factor can be derived as

$$M = \frac{n}{n_0} = \exp(\int_{r_1}^{r_2} \alpha(x)dx) \tag{27}$$

where x is the position of the charge in the counter.

The dependence of α on x comes through the E/p dependence and empirical expressions for the dependence of α on E/p have been given in literature :

$$\alpha = A\exp(-B/(E/p)) \tag{28}$$

where E and p are the electric field and gas pressure. Normally M is limited to $< 10^8$, after which electrical breakdown in gas occurs.

In a cylindrical proportional counter with the anode wire radius of a, and chamber radius, b, the induced voltages from electrons and ions at the anode can be written as

$$V^- = \frac{q}{2\pi\epsilon l}\ln(\frac{a+x_0}{a}) \tag{29}$$

$$V^+ = \frac{-q}{2\pi\epsilon l}\ln(\frac{b}{a+x_0}) \tag{30}$$

where q is the total charge released by ionization, l is the length of the chamber and is the distance from the wire at which the charges are produced.

The total voltage , $V = V^- + V^+ = -q/(lC)$

where $C = \ln\frac{b}{a}$ is the capacitance of the chamber per unit length.

The ratio of the contributions from electrons and ions to the total pulse height is

$$\frac{V^-}{V^+} = \frac{\ln\frac{a+x_0}{a}}{\ln\frac{b}{a+x_0}} \tag{31}$$

since typically, a = $10\mu m$, b = 10mm and $x_0 = 1\mu m$, the value of V^-/V^+ is 0.01. This means that the major contribution to the signal at the anode comes due to movement of positive ions in a cylindrical proportional counter.

The time development of the signal is given by

$$V(t) = \frac{-q}{4\pi\epsilon l}\ln(1+\frac{t}{t_0}) \tag{32}$$

where $t_0 = \frac{\pi P\epsilon a^2}{\mu C V_0}$

V_0 is applied voltage, μ is the ion mobility, P is the gas pressure in the counter. Due to low ion mobility, the signal rises slowly and in typical cases, it may take hundreds of microseconds to collect the full signal. However, one applies a short shaping time constant of the signal to derive pulses of microseconds duration.

3.1.3 Multiwire proportional chamber

A multiwire proportional chamber consists essentially of a set of thin, parallel and equally spaced abode wires, sandwiched between two cathode planes (fig.6). The gap,l, between anode and cathode is normally three to four times larger than the wire spacings. The voltages are applied in cathode and anode to operate the chamber in the proportional region. It was shown by Charpak and collaborators [4] that a multiwire proportional counter essentially acts as a set of independent proportional counters for each wire. Thus by locating the avalanche position by appropriate wire readout, it is possible to determine the position of interaction of the particle in the detector. The wire position readout is achieved electronically by any of the following methods : (i) delay line method, (ii) resistive method (iii) multiple sampling method. These type of chambers have been used extensively as position sensitive detectors for heavy ion research.

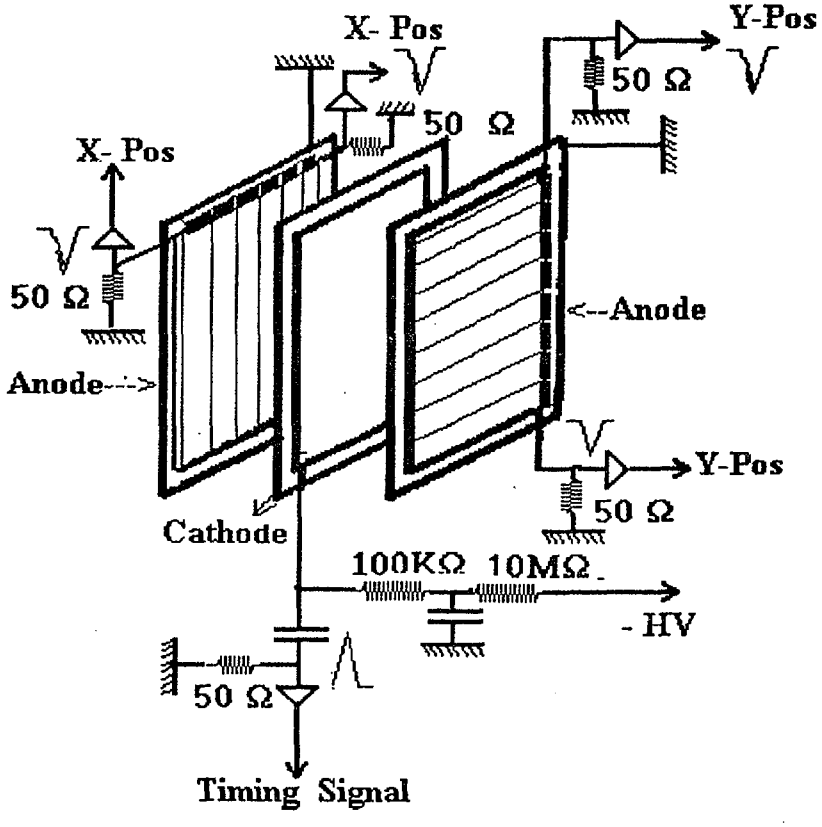

Figure 6: Multi-wire Proportional Counter

More detailed discussion on the multiwire proportional chambers and other types of gas detectors such as drift chambers, time projection chambers and cathode strip detectors

is beyond the scope of this article and the reader is referred to a large number of review papers and books that exist on this subject [5, 6, 7, 8].

3.2 Scintillation detectors

Certain materials when struck by a nuclear particle or radiation emit a small flash of light i.e. scintillation in a suitable wavelength region. Zinc sulphide as a scintillator in the visible wavelength region was used in the early periods of nuclear radiation studies. With the development of the photomultiplier tube by Curran and Baker [9] in 1944, the interest in scintillation detecters was resuscitated. Scintillators have many desirable general characteristics : (i) linearity to energy, (ii) fast time response, (iii) pulse shape discrimination and (iv) variety in materials (organic and inorganic types) etc. The light emission from scintillators can be characterised by the expression

$$N = A\exp(-\frac{t}{\tau_f}) + B\exp(-\frac{t}{\tau_s}) \tag{33}$$

where τ_f and τ_s are the fast and slow components and A,B are given by a functional form

$$A = N_0 f(\sigma, t) \tag{34}$$

$f(\sigma, t)$ being of a Gaussian shape. The ratio of the fast and slow components depends on the scintillator material and the type of radiation interacting with it. This property of certain scintillators for the dependence of the ratio of fast and slow components on the particle type helps in the identification of the nature of radiation by using the pulse shape discrimination techniques.

There are six types of scintillator materials namely : (i) organic crystals, (ii) organics liquids,, (iii) organic gases, (iv) inorganic crystals, (v) inorganic gases and (vi) inorganic glasses. We describe briefly below the main principles of the scintillation mechanism in the organic and inorganic materials and discuss the properties of some of the commonly used scintillation detectors for nuclear radiation detection.

3.2.1 Organic scintillators

These are aromatic hydrocarbon compounds containing linked or condensed benzene-ring structures. Scintillation arises from transitions made by free valence electrons of the molecules. These delocalised electrons are not associated with any particular atom in the molecule and occupy what are known as the π-molecular orbitals, consisting of spin singlet and spin triplet states as shown in fig.7. Molecules excited to higher excited states degrade to S_1 state without emission of light within < 10 ps (internal degradation). From S_1, there is high probability of radiative transition to S_0 states within a few nanoseconds time (fast component). The triplet states in a similar manner degrade to T_0 state by internal degradation, which then de-excites to S_0 indirectly through multiple collision process

$T_0 + T_0 \longrightarrow S^* + S_0$+phonons

and light comes after a delay time, which is characteristic of the interaction between the excited molecules (slow component) in the scintillator.

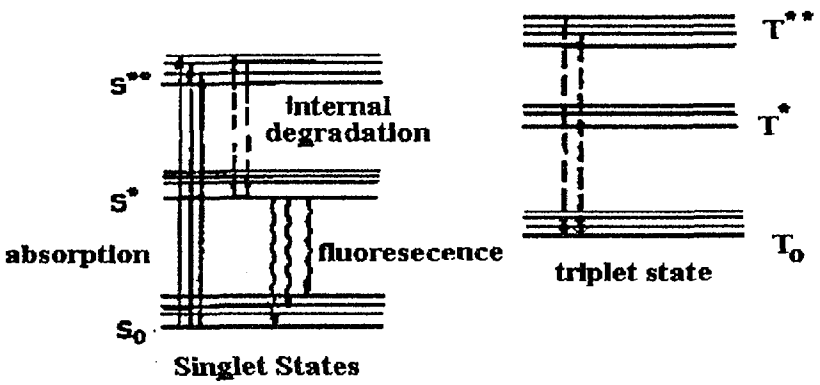

Figure 7: Deexcitation process in Organic Scintillators

Because of the molecular nature of the scintillation, the organic scintillators can be used in many physical forms such as crystals, liquids, plastics etc., without loss of scintillating properties. However, presence of small amounts of impurities can affect the light output significantly due to quenching. The scintillation efficiency is defined as the fraction of deposited energy that appears in the form of light radiation. The absolute efficiency of even the best organic scintillators is quite low (3.5% for anthracene, $C_{14}H_{10}$ as compared to 7% for NaI).

a. Organic crystals

Table 3 gives some of the properties of the organic crystals employed for radiation detection.

Crystal	decay time	light output
Anthracene,($C_{14}H_{10}$)	30 nsec	100% (normalised)
Trans-stilbene,($C_{14}H_{12}$)	4-5 nsec	50% - 75%
Naphthalene,($C_{10}H_8$)	few nsec	30% - 40%
p,p'- quarterphenyl	7.5 nsec	90%

Table 3.

The main drawback in the organic crystals is the anisotropic response due to channelling effects.

b. Organic liquids

The organic liquid scintillators are made by dissolving the scintillation solute in an organic solvent liquid. Ionisation energy is absorbed mainly in the solvent and then passed on to the scintillating solute. The solvents commonly used are : xylene, toluene, benzene, phenylcyclohexane, triethylbenzene and decaline etc. The organic scintillator solutes are :

p - Terphenyl ($C_{18}H_{14}$)

PBD (2-phenyl, 5,(4-biphenyl) - 1,3,4 - Oxadiazole) ($C_2H_{14}N_2O$)

PPO (2,5-diphenyl oxazole) ($C_{15}H_{11}NO$)

POPOP (1,4-Bis-[2-(5-phenyloxazolyl)] - benzene) ($C_{24}H_{16}N_2O_2$)

The efficiency of liquid scintillators increases with solute concentration before reaching a broad maximum before saturation of solution takes place. Typical concentrations are 3 gm of solute per litre of solvent. The scintillation decay times are typically 3 to 4 nsec. The advantages of the liquid scintillators are the following:

i) possibility of loading of other elements for specific detector applications: ^{6}Li, Gd, ^{11}B for neutron and Sn, Pb for γ-rays

ii) loading of wavelength shifters for matching to PM tube

iii) pulse shape discrimination due to different response for different ionising particles.

The disadvantages are that the light output is extremely sensitive to impurities, such as dissolved oxygen and other elements. Normally oxygen can be removed bubbling dry N_2 gas. Quenching due to loaded impurities can be minimized by adding naphthalene, biphenyl etc. to the solvent.

c. Plastics

These types of organic scintillators are most widely used due to their flexibility in machining, robustness, size and thickness. Plastic scintillators are also solutions of organic scintillators in a solid plastic solvent such as polyvinyltoluene (PVT), polyphenylbenzene (PPB) and polystyrene . The primary solutes are PBD and p-terphenyl ($\sim 10gm/l$) and secondary solute is POPOP which is used for wavelength shifting to match with PM tube response. The typical scintillation decay times are in the range of 1-3 nsec in most plastic scintillators, which makes them quite suitable for fast timing applications.

3.2.2 Inorganic scintillators

Certain halides, fluorides and oxides containing sometimes small amounts of activator impurities act as scintillators. The spectrum of the emitted light is in the range of 200nm - 600nm. In general, inorganic scintillators are 2-3 orders of magnitude slower in response than organic scintillators due to phosphorescence (CsF, however, has a fast decay time of ~ 5 nsec). Major disadvantage for some inorganic scintillators is hygroscopicity. The advantage of inorganic scintillators over organic scintillators is the greater stopping power to gamma rays due to their higher density and higher atomic number.

The scintillation mechanism in inorganic crystals is characteristic of the electronic band structure transitions. The doping of impurities helps in shifting the wavelength of light emission to the suitable range for matching to the response of the photomultiplier tubes. The light output response varies from scintillator to scintillator, and also depends on the type of particles causing the ionisation. In certain scintillators, there is a slow and fast component, whose relative magnitude depends on the density of primary ionization. This property has been exploited to carry out particle identification by pulse shape discrimination technique. The characteristics of various types of inorganic scintillators developed for nuclear particle detection have been listed in table 4. Certain high Z oxide based scintillators such as BGO, $CdWO_4$ etc. have been recently developed and have very good stopping power to gamma rays due to their high densities. The light output decides the energy resolution achievable with different types of scintillators. Depending on the applications with regard to the requirements of energy and timing resolutions, counting rates, detection efficiency and particle identification by pulse shape discrimination, one can select the type of detector material best suited for a particular experimental set up.

Detector material	Density (gm/cc)	Decay time (nsec)	Wavelength of emission (nm)	Light yield (%)	Hygroscopic
NaI(Tl)	3.67	230	415	100	Yes
CsI(Tl)	4.53	1000	550	85	slight
CsI(pure)	4.53	2.2-20	305	6	slight
		1000	400		
LiI(Eu)	4.08	1400	480	35	yes
CaF_2(Eu)	3.19	940	435	50	no
BaF_2	4.9	0.6	220	20	no
		620	310		
CeF_2	6.16	5	310	5-10	no
GSO $(Gd_2SiO_5;Ce)$	6.71	60	430	20	no
BGO $(Bi_4Ge_3O_{12})$	7.13	300	480	12	no
$ZnWO_4$	7.87	5000	480	26	no
$CdWO_4$	7.90	5000	540	40	no

Table 4.

3.3 Semiconductor detectors

Development of these detectors were started during 1950s and these detectors became commercially available in 1960s. Due to certain desirable features such as good energy resolution, higher density compared to gas and good time response, these detectors are increasingly being used for nuclear spectroscopy applications. The most common semiconductor detectors are made of silicon and germanium. The band gap in these materials are 1.1eV and 0.7eV respectively, which governs the amount of energy required to create an electron-hole pair. Silicon detectors are better suited for room temperature applications for charged particle detection, whereas germanium detectors are preferably used at LN2 temperature for gamma ray detection purpose.

The detectors are made by having a semiconductor with np junction and by applying the operating voltage in the reverse bias mode. In this mode, a depletion zone is formed which is free of charge carriers and possesses a linearly varying electric field as shown in fig.8. The depletion depth depends on the concentration of n and p impurities and the applied voltage.

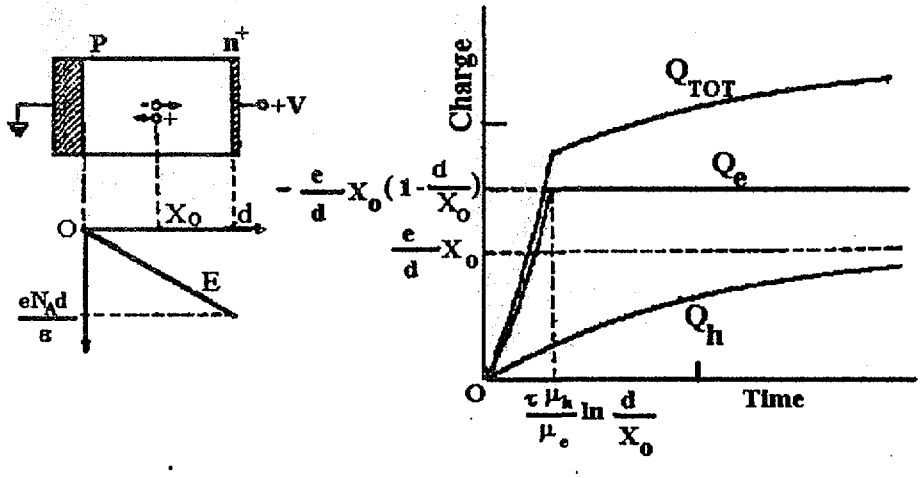

Figure 8: Signal pulse shape in a np junction

In terms of resistivity of the bulk material, one can write the relationship for the depletion depth as a function of applied reverse bias voltage as follows :

$d = 0.53(\rho_n V_0)^{\frac{1}{2}}\ \mu m,$ for Si n-type

$= 0.32(\rho_p V_0)^{\frac{1}{2}}\ \mu m,$ for Si p-type

The junction capacitance can be calculated as follows :

$$C = 2.2(\rho_n V_0)^{-\frac{1}{2}}\ pF/mm^2, \quad \text{for Si n-type}$$

$$= 3.7(\rho_p V_0)^{-\frac{1}{2}}\ pF/mm^2, \quad \text{for Si p-type}$$

The energy resolution achievable with Si-semiconductor detectors is again decided by w, the average energy required to produce an electron-hole pair, which is about 3.62 eV at T= 300^0K. By using the Fano factor of 0.12, one can see that for 5 MeV α-particles, the FWHM is about 3.5 keV due to statistical spread in the e-h production. The observed energy resolution is ,however, dominated by the electronic noise of the pulse processing modules and one normally gets typical resolutions of 20-25 keV for the semiconductor detectors at room temperature. There are various types of detectors made for charged particle spectroscopy applications, depending on the method of creating the semiconductor junction and the depletion zone. These are :

i) Diffused junction : The junction is made by diffusing n and p type impurities from the two sides. The concentrations of n- and p-types are controlled to provide the suitable depletion layer containing the electric field for collection of ionisation charges due to incident radiation.

ii) Surface barrier : The junction is formed by evaporating a metal on a semiconductor. The barrier so formed is called Schottky barrier. For n-type Si, gold provides the surface barrier junction, whereas for p-type Si, aluminium provides the surface barrier junction.

iii) Ion implanted diode : In this case the impurity atoms are implanted into the silicon crystal with a low energy (50-100 keV) ion implanter. Both boron and phosphorous atoms can be used for n-type and p-type materials to provide the junction.

iv) Li-drifted Si-diode or Si(Li) detector : This is based on the compensation of the impurities of the base material, to provide large thickness for the depletion zone. Large intrinsic layer thicknesses of 3-5 mm can be achieved by this process. Such detectors are widely used for x-ray detection in the energy range of 1-100 keV, after cooling the detector and the first FET stage of the preamplifier to liquid nitrogen temperature. In this way, energy resolutions of 150-200 eV can be achieved for 5.9 keV ^{55}Fe X-rays to carry out high resolution energy dispersive x-ray measurements.

v) High purity germanium detectors : For gamma ray detection, germanium is preferred over silicon due to its much higher atomic number. In order to obtain a sufficient sensitive thickness for detection of high energy gamma rays, earlier the detectors were made from lithium compensated p-type germanium. However, these detectors have to be kept continuously cooled at liquid N2 temperature, due to high mobility of Li ions in germanium at room temperature. Recently, it has been possible to grow germanium crystals with very high purity such that the impurity concentrations are less than 10^{10} atoms/cc. Detectors made out of such crystals do not need any Li compensation and are called high purity germanium detectors. One advantage of this is the possibility of using n-type germanium, where

a very thin window can be formed by ion implantation to extend the sensitivity to very low energy gamma rays. Presently, Ge detectors are available with large volume crystals having good photopeak efficiency for MeV gamma rays. However, in order to further reduce the Compton scattered background from the gamma ray spectra, one employs a scintillation based Compton shield around the Ge detector, which is operated in anti-coincidence mode with the Ge detector. Such Compton suppressed high purity Germanium detectors are used extensively for high resolution spectroscopic studies in nuclear physics research.

As one can see from above, semiconductor detectors are available in wide varieties for energy spectroscopy of charged particles and gamma rays. More recently, due to advances in silicon processing technology, very high resolution position sensitive detectors are being made which can provide position resolution in micron range for particle tracking in high energy physics experiments [10].

4 Cherenkov Radiation and Cherenkov Counters

Cherenkov radiation occurs when the velocity of a charged particle traversing a material medium exceeds the velocity of light in that medium. The cherenkov photons are emitted at a fixed angle, which is decided by the velocity of the particle and the refractive index, n of the medium as

$$\cos\theta = \frac{1}{\beta n} \ , \ \beta = \frac{v}{c}$$

The velocity threshold for Cherenkov radiation in a medium is, therefore, $\beta_{th} = \frac{1}{n}$. It may be noted that for a given medium, n is a function of wavelength λ as well as temperature of the medium.

The amount of energy radiated in Cherenkov radiation per unit length per unit frequency interval $d\omega$ by a particle of charge ze is given by

$$\frac{dE}{dxd\omega} = \frac{z^2 r_e m_e c^2}{c^2}(1 - \frac{1}{\beta^2 n^2})\omega \tag{35}$$

for z = 1 and expressing $\omega = \frac{2\pi c}{\lambda}$, we get

$$\frac{dE}{dxd\lambda} = \frac{4\pi r_e m_e c^2}{\lambda^3}(1 - \frac{1}{\beta^2 n^2}) \tag{36}$$

The emitted energy is strongly peaked at short wavelengths.

In practice, the condition $\beta n > 1$ is only satisfied for the ultraviolet to near infrared portion of the electromagnetic spectrum. If the variation in $n(\lambda)$ is small over the wavelength region λ_1 to λ_2 , the energy radiated per unit path length becomes,

$$\frac{dE}{dx} = 2\pi^2 r_e m_e c^2 \sin^2\theta(\frac{1}{\lambda_1^2} - \frac{1}{\lambda_2^2}) \tag{37}$$

and the photon yield ($N = E/(h\nu)$) is given by

$$\frac{dN}{dx} = 2\pi\frac{e^2}{\hbar c}\sin^2\theta(\frac{1}{\lambda_1} - \frac{1}{\lambda_2}) \tag{38}$$

For example, using the wavelength interval of 400 - 500 nm, one gets

$$\frac{dE}{dx} \sim 640\sin^2\theta \text{ eV/cm and } \frac{dN}{dx} \sim 220\sin^2\theta \text{ photons/cm}$$

Taking n = 1.33 and $\beta \sim 1$, one gets $\theta = 41.2^0$, which implies that about 300 eV/cm is given off as Cherenkov radiation in this wavelength region. It may be noted that this is quite small compared to the $\sim$ 2 MeV/cm ionisation energy loss and about 100 times weaker than the light output from a plastic scintillator. However, due to certain distinguishing characteristics such as instantaneous emission, δ -function in angular distribution etc., Cherenkov radiation is used in many important applications.

Since the light yield from Cherenkov radiation is very small, extreme care has to be taken to collect as many photons as possible. Cherenkov radiator should be transparent to the emitted radiation over the desired wavelength range. The radiator should not produce scintillation light, and should have small density and atomic number in order to minimize ionisation loss and multiple scattering. The light collection system should be as efficient as possible. The optics should be designed to minimize light loss in reflections and transmission through windows etc. High quality photomultiplier tubes are necessary for single photon detection.

Various types of Cherenkov counters have been employed, especially in experiments in high energy physics. Depending on the type of application and construction features, these counters can be classified as follows and are shown schematically in figs. 9(a) - 9(c).

i) Threshold counters

Since Cherenkov radiation is produced only when the velocity of a particle exceeds a minimum value $\beta_{th} = 1/n$, such counters can be used as threshold devices to indicate the presence of a particle with velocity greater than a certain minimum value. In a beam of fixed momentum, sets of such counters can be used to identify particles with different masses. Fig.9(a) shows a schematic diagram of such a counter.

ii) Differential counters

A differential counter can measure the velocity of a particle by only accepting Cherenkov light in a small annulus around some angle (fig.9(b)). Using such a counter, it is possible to provide a signal for the presence of a given mass particle.

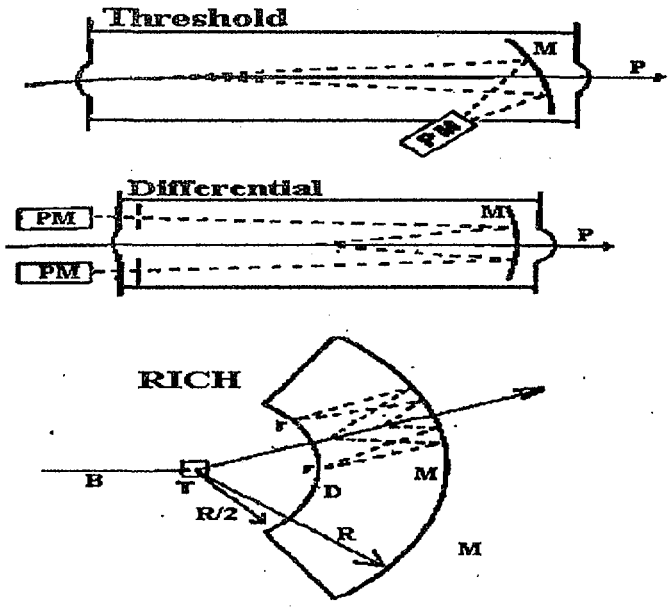

Figure 9: Schematic diagram of different types of Cherenkov Detectors

iii) Ring imaging Cherenkov counter (RICH)

This is an extension of the differential counter. The radiating medium is contained between two spheres surrounding the target or intersection point. The Cherenkov light reflects off the mirror(M) and is focused onto a ring at the detector surface (D). With this geometry the radius of the ring(r) is directly related to the Cherenkov angle (θ) by

$$r = f \tan\theta \tag{39}$$

where f is the focal length of the mirror. The radius of curvature(R) of a spherical mirror being 2f, the detector plane is kept at the radius R/2 as shown in fig.9(c). RICH counters are also quite useful in π/e separation in high energy physics experiments by using gas radiators which are tuned to produce Cherenkov radiation only for large β values which correspond to electrons emitted in the collisions at relativistic energies. Recently, such detectors have been used in the PHENIX heavy ion experiment, which we shall describe later.

iv) Total absorption counter

In a total absorption Cherenkov counter, the incident particle energy is fully deposited in the detector medium. Such counters have been used to measure the energy of photons or electrons by creating an electromagnetic shower hrough the combined processes of bremsstrahlung and pair production, which we will discuss in a later section. Lead glass has been used to make such detectors. In other applications, neutrino detection can be done through secondary electron productions in weak interactions, which are detected by the Cherenkov process. The Kamiokande detector in Japan is a good example for such a detector.

5 Electromagnetic Calorimeters

For high energy photons (E_γ > a few tens of MeV), the major interaction in a detector medium is by pair production and for electrons with similar energy bremsstrahlung process is the dominant mode of energy loss. In both these processes, the initial energy of the photon or the particle gets reduced on the average by a factor of two after each interaction. These two processes continue alternately producing an electromagnetic shower. The length of a shower depends on the initial energy of the photon and can be calculated in an approximate manner as follows:

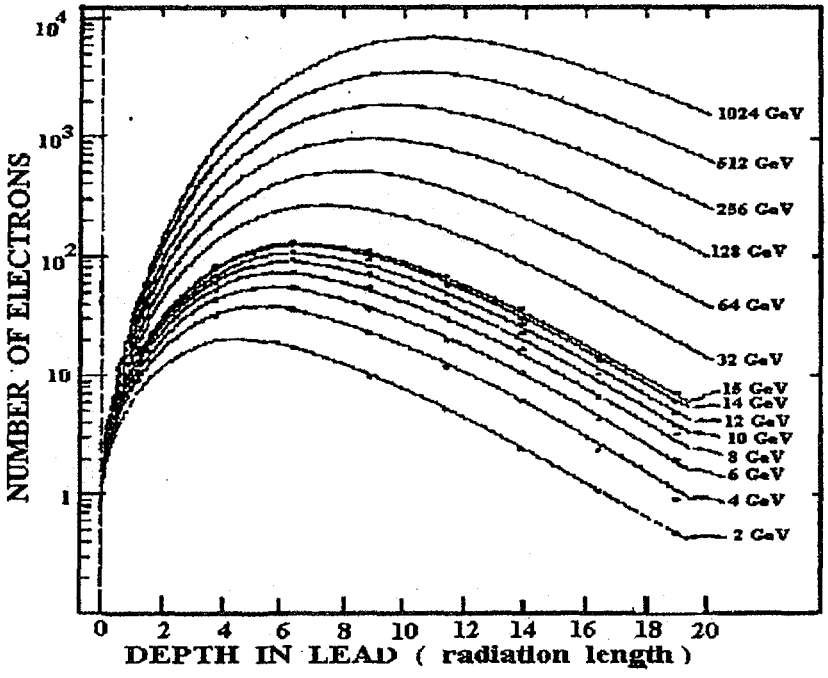

Figure 10: Longitudinal profile of e.m. shower

Let E_0 be the initial energy. After one radiation length,X_R the photon on an average gets converted to an e^+, e^- pair each having energy $E_0/2$. After two X_R, the e^+, e^- will each emit a bremsstrahlung photon with approximately half the energy of the charged particle. After t radiation lengths, total number of particles (photons, e^+ and e^-) will be $N \approx 2^t$ with average energy $E \approx E_0/2^t$. If we assume that shower stops at the critical energy E_c, then

$$E(t_{max}) = E_c = \frac{E_0}{2^{t_{max}}} \tag{40}$$

or

$$t_{max} = \frac{\ln \frac{E_0}{E_c}}{\ln 2} \tag{41}$$

and

$$N_{max} \approx \frac{E_0}{E_c} \tag{42}$$

In reality, the number of particles in an e^+, e^-, γ cascade rises exponentially to a broad maximum after which it declines gradually as shown in fig.10. Empirical fits to the Monte Carlo simulations for the shower profile yield the following relations for the shower path length and number of particles at the shower maximum.

$$t_{max} = 3.9 + \ln E_0(GeV) \tag{43}$$

$$N_{max} = 8.46\ E_0^{0.935} \tag{44}$$

The longitudinal development of electromagnetic showers in different materials is found to scale if the distances are measured in radiation lengths.

Another quantity of interest in an e.m. shower is the shower radius. The radius within which 90% of the shower particles are contained at each depth is called the "Moliere Radius", which is approximately given by $\rho \simeq 7A/Z\ \ g/cm^2$. Roughly, 95% of the shower is contained laterally in a cylinder with radius $2\rho_m$. The transverse shower profile as a function of shower depth clearly exhibits rather pronounced central and energetic core surrounded by a low energy halo.

An electromagnetic calorimeter can be conceptually thought to be a block of matter that is of sufficient thickness to cause an interacting particle deposit all its energy inside its volume. A fraction of the deposited energy is detectable in the form of a more practical signal (e.g. scintillation, Cherenkov light or ionisation charge etc.), which is proportional to the initial energy. The uncertainty in the energy measurement is governed by statistical fluctuation in the average number of secondary particles. Hence,

$$\frac{\sigma}{E} \sim \frac{1}{\sqrt{N}} \sim \frac{1}{\sqrt{E}} \tag{45}$$

The length of the detector to stop particles of energy E increases logarithmically with particle energy.

There are two types of calorimeters : a) homogeneous and b) sampling. The homogeneous calorimeters are made by large volume detectors of single type. For very high energy particles, sampling calorimeters are usually employed, which consist of alternate layers of high-Z converter material and low-Z detector material. A small fraction of the shower energy is sampled. The advantages of sampling calorimeters are i) possibility of both longitudinal and lateral segmentation ii) economy of detector size and iii) low cost. The factors which affect the energy resolution in the sampling electromagnetic calorimeters are i) leakage of the shower ii) sampling fluctuations iii) Landau fluctuations and iv) path length fluctuations.

Given sufficiently fine grained instrumental resolution , the localisation of the centre of gravity of the transverse distribution of the shower profile can be achieved by sampling the initial part of the shower.

6 Particle identification techniques

One of the important requirements of a detector setup is to identify the type of particles entering the detector medium. Various methods have been employed depending on the particle type and energy range to be investigated and on the requirement for the resolution with which they have to be measured. These methods are broadly based on the following principles.

i) Energy loss
ii) Pulse shape analysis
iii) Time of flight
iv) Magnetic spectrometry

As we have seen earlier, the energy loss of a charged particle in a detector medium can be written as

$$\Delta E \ \alpha \ \frac{MZ^2}{E} \tag{46}$$

where M, Z and E are the mass, charge and energy of the particle. If one measures simultaneously the E and ΔE of the particle, one can derive the information on the product MZ^2 of the particle. This method is widely employed for identification of light and medium heavy nuclei produced in nuclear collisions. The ΔE and E of the particle can be measured by employing a detector telescope consisting of a thin detector followed by a thick detector to completely stop the particle. The two detectors can be combination of any of the types such as gas, semiconductor and scintillation detectors. In some situations, two scintillation detectors having different decay times are used in sandwich geometry and are read out by a single photomultiplier tube. By selecting suitable integration times for the observed signal, it is possible to derive the $\Delta E, E$ information from such a device. This type of assembly is known as phoswich detector assembly and has been used in many experimental setups for charged particle spectroscopy studies.

Another method of particle identification is the pulse shape analysis from a single detector. As mentioned above, many scintillators have both slow and fast decay times of the scintillation ionisation density in the detector medium. The inorganic scintillators, CsI, BaF_2, NaI and certain types of organic scintillators such as NE213 possess this property. Recently, the rise time differences in the pulse formation in semiconductor detectors have also been exploited to carry out particle identification by pulse shape analysis. It has been shown that by allowing particles to enter from the ohmic contact side improves the quality of pulse shape discrimination in these detectors. An example of the pulse shape discrimination with silicon ΔE detectors is shown in fig.11. This principle has been exploited in making large detector setups for various experimental studies. One major experimental facility using the PSD principle for silicon detectors is the 8π LP detector array set up at the Legnaro

National Laboratory in Italy. This detector array consists of 262 ΔE - E telescopes arranged around the target to cover 90% of 4π for detection of light cahrged particles. More details of this set up can be found in ref [11].

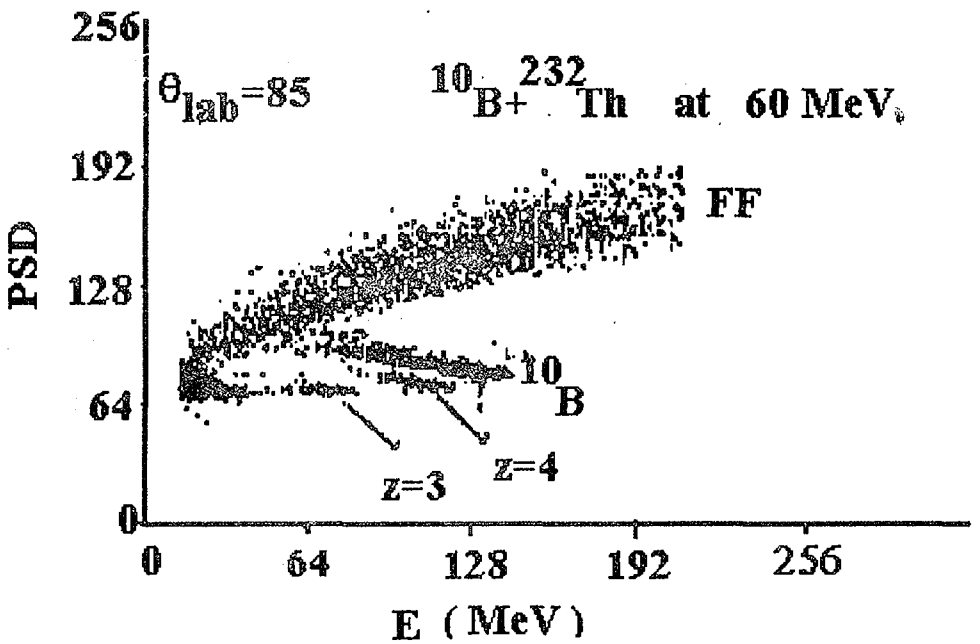

Figure 11: Pulse shape Vs Energy in a Surface Barrier Detector

The time of flight method for particle identification uses the relations

$$TOF = \frac{d}{v}; \quad v = \sqrt{\frac{2E}{M}} \tag{47}$$

By measuring the energy and time of flight, one can determine the mass of the particle entering the detector. This method has been also used extensively for neutron energy measurements using fast liquid scintillators, where gamma-neutron discrimination is carried out by pulse shape analysis and neutron energy is determined from the time of flight of the neutrons.

In magnetic spectrometry, the particles are made to traverse in a magnetic field. The deflection in the trajectories of the particles depends on their momentum. In a uniform field, one can use the relations

$$p = mv = Bq\rho \tag{48}$$

and

$$E = \frac{p^2}{2m} \tag{49}$$

By simultaneous measurement of energy and radius of curvature ,ρ one can derive the information on the mass of the particle. However, in a non-uniform magnetic field, one needs to integrate the above expression to determine the deflection of the particle as function of its momentum. These different methods have been employed in suitable combinations to carry out particle identification and energy measurements in various detector setups. A review on the charged particle detector arrays built in different accelerator laboratories can be found in ref [12].

In the following section, we shall briefly describe one of the most advanced and complex detectors(PHENIX) being set up for heavy ion collisions at relativistic energies at the RHIC accelerator at BNL, USA. This detector provides a good example as to how different detection principles are employed to carry out the measurements in an environment of very high particle multiplicities produced in relativistic heavy ion collisions.

7 PHENIX Detector

The PHENIX detector is being set up at the Relativistic Heavy Ion Collider (RHIC) at BNL, USA to study the p-p, p-A and A-A collisions upto few hundred GeV/n centre of mass energy. The RHIC accelerator, when operational by the middle of 1999, will be the highest energy accelerator for heavy ions and will be used to investigate the possibility of the phase transition of normal nuclear matter to quark gluon plasma at extremely high temperatures and matter densities. The signatures for such a phase transition have been predicted theoretically in terms of changes in the properties of vector mesons ($\rho, \omega, \phi, J/\psi, \psi'$ etc), enhancement in the production of strange and charm particles, particle correlations and changes in the ratio of the yields of various baryons and mesons etc. The PHENIX (Pioneering Heavy ion Interaction Experiment) experiment has been designed to measure with good efficiency and resolution, these various quantities in the high multiplicity environment of the heavy ion collisions at the relativistic energies. The PHENIX detector consists of detector elements to measure the leptons (e^+, e^-, μ^+, μ^-) ,which are emitted as decay products of the primary particles as well as photons and hadrons produced during the collision process. Fig.12 shows the layout of the PHENIX detector. This consists of two central electron arms and two end to end muon arms. Apart from these detectors, there are inner detectors such as beam-beam counters along the beam pipe and silicon vertex detectors arranged around the collision point. The momentum dispersion of the particles is done by the central magnet having field in axial direction and the muon magnets having field along radial direction. In the following, we give a description of the salient features of the different detector elements of the PHENIX detector.

7.1 Inner Detectors:

7.1.1 Beam-Beam counters:

The two sets of beam-beam counters are arranged along the beam axis symmetrically on either side of the beam collision region. The counters are made of Pb-Glass Cherenkov detectors, which provide very fast timing signals and enable the determination of the space-time location of the collision point for first level trigger purpose. A position resolution of about 2 cm in z-direction of the collision point is achieved by these detectors. The timing resolution is obtained as 60-80 picosec by using very fast photo-multiplier tubes to detect the Cherenkov radiation from the BBC detectors.

7.1.2 Vertex Detectors:

This consists of three layers of thin microstrip detectors having very large granularity and good position resolution. The radiation length of these detectors is very small and is not sufficient to initiate e-m showers for the electrons and photons. The particle tracks generated out of the hits in these detectors are extrapolated into the collision region to reconstruct the vertex location to an accuracy of about 100-200 microns. Such a precise determination of the collision vertex improves the momentum resolution of the particle tracks in the tracking detectors.

7.2 Electron Arm :

The electron arms consist of a number of gas tracking detectors of drift chamber and pad chamber design to construct the particle tracks, and at the end the electro-magnetic calorimeters are placed to determine the total energy of the particles. There are also ring imaging Cherenkov counters, which are highly useful to discriminate electrons from the hadrons. RICH detectors play a key role as trigger detectors in PHENIX experiment since they can effectively eliminate the large background of pions with about $10^4 : 1$ ratio, thereby providing a clean set of signals for the electrons and photons. With the combination of momentum from the tracking detectors and total energy from electromagnetic calorimeters, one can identify the electrons from other type of particles. The e-m calorimeters in the PHENIX detector are mainly of sampling type which are highly segmented to determine the location of the interaction point. The particle tracks generated in the tracking detectors are connected with the e-m calorimeter to correlate their signals. The electron arms also contain a small coverage for detecting hadrons like pions, kaons etc through the use of time of flight detectors. These detectors are made of scintillator blocks, which are coupled to PM tubes for giving the time of interaction. By combining the time of flight and momentum information, the mass of hadrons are determined. Thus by a combination of varieties of detector types in the electron arm, one is able to measure the very weak electron signals in the presence of a large background of hadrons produced in the relativistic heavy ion collisions.

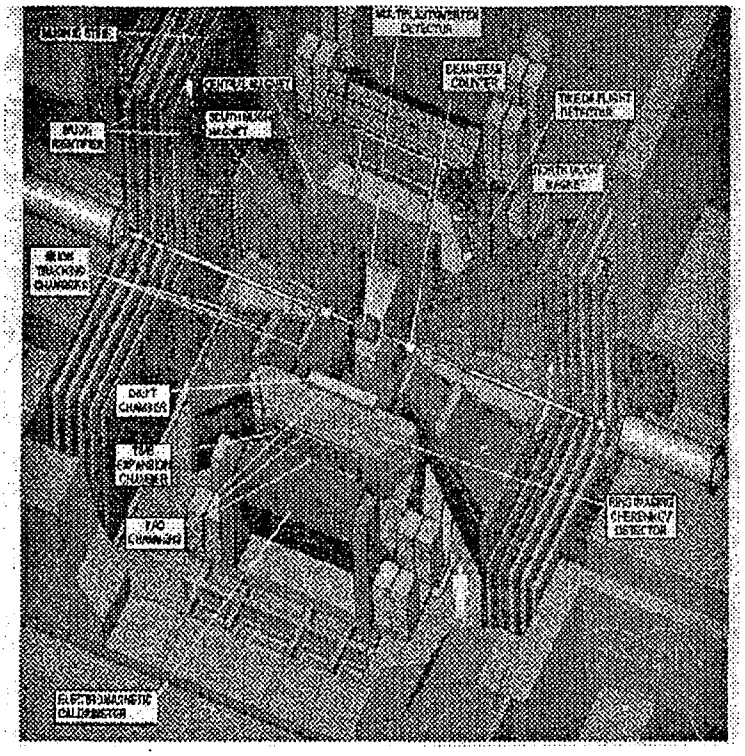

Figure 12: Schematic layout of the PHENIX detector

7.3 Muon Arm:

Muons are identified mainly by the fact that they have the least stopping in any medium compared to electrons and hadrons. The first elements in the muon arms are the thick absorbers of the central magnet pole piece, which largely stop the electrons and hadrons but preferentially allow muons to pass through. The particles penetrating these absorbers are mainly muons with a small fraction of energetic hadrons. These particles are then bent in the magnetic field to determine their momentum and at the end again pass through a series of Fe absorbers interfaced with gas streamer tube detectors to identify them as muons. The μ^+ and μ^- pairs detected in the muon arms can be correlated to construct the invariant mass of the emission source of the muons.

The above discussion of the PHENIX detector was meant to mainly illustrate the use of various detection methods and techniques to carry out very complex measurements in the relativistic heavy ion collisions. It is,however,not possible to go into further details of the design and performance characteristics of the different types of detectors used in the PHENIX experiment, within the scope of the present write up.

8 Summary

This lecture series was aimed at providing a basic understanding of the detection principles employed in nuclear physics studies. Detectors are made by exploiting different aspects of the particle interactions in the medium. The modern detector systems are highly complex and modular, trying to achieve the ultimate performance in resolution and sensitivity. Apart from the detectors,it is also the signal processing electronics which go together to bring out the best in the performance of the experimental setups.

We have not been able to touch upon the advances made in the electronics and data processing systems that have taken place in the recent times. Also the wide range of position sensitive detectors with wide range of applications in other areas of science could not be covered in the present lectures and the reader may refer to many books and review articles available in the literature on these detectors.

References

[1] N.Bohr, Kgl.Danske Videnskab. Selskab, Mat. Fys. Medd. 18(1948)8

[2] See S.Ahlen, Rev. Mod. Phys. 52(1980)121

[3] See H.A.Bathe and J.Ashkin, Passage of radiation through matter in E.Segre (Ed.) Experimental Nuclear Physics Vol.1, Part 2, New York, Wiley (1959)

[4] G.Charpak, R.Bouclier, T.Bressani,J.Favier and C.Zupanacic, Nucl. Instr. Meth. 62(1968)235

[5] G.Charpak and F.Sauli, Proc. Conf. on computer-assisted scanning, Padova,21-24 April (1976), p 592

[6] F.Sauli ,"Principles of operation of Multiwire Proportional and Drift Chambers", CERN Report 77-09 (1977)

[7] M.Atac and W.E.Taylor, Nucl. Inst. & Meth. 120(1974)147

[8] K.Kleinknecht, "Particle Detectors" in Techniques and concepts of High Energy Physics, ed. by T.Ferbol (Plenum Press, New York 1981)

[9] J.M.Schonkeren, "Photomultipliers", Philips Application Book Series ed. H.Kater and L.J.Thompson (Philips Eindhoven, The Netherlands)(1970)

[10] B.Hyams, U.Koetz, E.Belau, R.Klanner, G.Lutz, E.Neugebarcer, A.Wylie and J.Kemmer, Nucl. Inst. & Meth. 205(1983)99

[11] G.Prete, E.Fioretto, M.Cinausero, M.Giacchini, M.Lollo, D.Fabris, M.Lunardon, G.Nebbia, M.Caldogonom, A.Brondi, G.LaRana, R.Moro, E.Vardaci, A.Ordine, A.Zaghi, A.Boiano, P.Blasi, N.Gelli, F.Lucarelli, G.J.Yuan and B.K.Nayak, Nucl.Inst. & Meth. A422(1999)263

[12] R.K.Choudhury , Proc. IV SERC school on Intermediate Energy Nuclear Physics, Goa, Ed. Y.K.Gambhir(1993)

Published by : Dr. Vijai Kumar, Head Library & Information Services Division
Bhabha Atomic Research Centre, Mumbai - 400 085, India.